AIAA JOURNAL
Vol. 34, No. 11, November 1996

Combined Laser Doppler Velocimetry and Cross-Wire Anemometry Analysis for Supersonic Turbulent Flow

Rodney D. W. Bowersox*
U.S. Air Force Institute of Technology, Wright–Patterson Air Force Base, Ohio 45433-7765

A synergistic laser Doppler velocimetry and multiple overheat cross-film anemometry analysis was developed to allow for direct measurements of the mean and turbulent flow properties in a supersonic turbulent flow. The present technique facilitated, for thin-layer, nonreacting flows, the measurement of the Reynolds (time) and Favre (mass-weighted time) averaged turbulent shear stress, heat flux, and apparent mass flux, without the usual ad hoc assumption of negligible static pressure fluctuations. The mean velocity, mass flux, and density were also acquired. The directly measured mean flow and turbulence results, in a Mach 2.8 wall boundary layer ($Re_\theta = 1.12 \times 10^4$), were found to compare very well with numerical predictions based on the k-ω two-equation (for the Favre approach) and the compressible apparent mass mixing length extension algebraic (for the Reynolds approach) turbulence models.

Nomenclature

C_p = specific heat at constant pressure
d_w = hot-film (wire) diameter
h = enthalpy
M = Mach number
Nu = Nusselt number
OHR = overheat or resistance ratio, R_w/R_o
p = pressure
R = resistance
Re = Reynolds number
S = compressible apparent mass mixing length extension model constant, 1.0
T = temperature
U = mean Favre axial velocity
u, v = velocity components
u^* = friction velocity
x, y = Cartesian coordinates
y^+ = $\rho_w u^* y/\mu_w$
δ = boundary-layer thickness
δ^* = compressible displacement thickness
δ_k^* = kinematic displacement thickness
γ = ratio of specific heats, 1.4
θ = $\overline{\rho v}/\overline{\rho u}$
θ_k = kinematic momentum thickness
μ = viscosity coefficient
ρ = density

Subscripts

c = cone static pressure
e = effective
L = lead
o = reference condition
r = recovery
S = top, $R_S = 50\ \Omega$
t = total condition
w = wire (film) or wall
2 = behind a normal shock

Superscripts

F = Favre
o = outer region of the boundary layer
R = Reynolds
T = Turbulent
$\overline{\ }$ = time average
$'$ = Reynolds fluctuation
$''$ = Favre fluctuation

Received Feb. 9, 1996; revision received July 22, 1996; accepted for publication July 22, 1996; also published in *AIAA Journal on Disc*, Volume 2, Number 1. This paper is declared a work of the U.S. Government and is not subject to copyright protection in the United States.

*Assistant Professor, Department of Aeronautical and Astronautical Engineering, Graduate School of Engineering. Member AIAA.

Introduction

As a result of analytical and numerical intractability, the current understanding of supersonic turbulent flows is founded heavily in experimental observation and reasonable extrapolation[1] from the relatively vast low-speed database. Because of the difficult nature of obtaining turbulence measurements in supersonic flow,[2] the quantity and quality of the available data are very limited.[3] Compounding the dilemma is the fact that the flow regime where Morkovin's hypothesis is valid, which states that the essential dynamics of supersonic turbulent boundary layers follow the incompressible pattern, and is the basis for the extension of the subsonic analyses to supersonic flow, has proven to be more limited than originally believed.[2]

Since direct numerical and large eddy simulation of practical high Reynolds number supersonic flows is well beyond the current state of computational capabilities, engineers and scientists have relied on an approximate averaged form of the Navier–Stokes equations. Reynolds and Favre averaging are the two prevalent techniques. This procedure results in additional fluctuation cross correlations terms that appear in the averaged form of the governing equations. The presence of these terms, which require modeling, defines the closure problem in turbulence. The Reynolds averaged turbulence properties are given by

$$m_i^R = -\overline{\rho' u_i'}$$

$$\tau_{ij}^R = -\bar{\rho}\overline{u_i' u_j'} - \bar{u}_i\overline{\rho' u_j'} - \bar{u}_j\overline{\rho' u_i'} - \overline{\rho' u_i' u_j'} \tag{1}$$

$$q_i^R = \bar{\rho}\overline{h_t' u_i'} + \bar{h}_t\overline{\rho' u_i'} + \bar{u}_i\overline{\rho' h_t'} + \overline{\rho' u_i' h_t'}$$

The turbulent mass flux m_i^R, shear stress τ_{ij}^R, and heat flux q_i^R are associated with the conservation of mass, momentum, and energy, respectively. The corresponding Favre averaged quantities are given by

$$m_i^F = 0$$

$$\tau_{ij}^F = -\bar{\rho}\overline{u_i'' u_j''} - \overline{\rho' u_i'' u_j''} \tag{2}$$

$$q_i^F = \bar{\rho}\overline{h_t'' u_i''} + \overline{\rho' u_i'' h_t''}$$

where, for nonreacting flows, the triple correlation terms are usually neglected.

Over the years, hot-wire anemometry, especially the normal wire, has emerged as the primary tool for supersonic turbulent

research.[4–15] In supersonic flow, the hot-wire signal is a function of both instantaneous mass flux and total temperature. However, these variables do not directly appear in either the Reynolds or Favre averaged Navier–Stokes equations [Eq. (1) or (2)]. Hence, the static pressure fluctuations are usually neglected to decompose the hot-wire results into a more conventional form.[7] Although it has been argued that the static pressure fluctuations are small for moderate supersonic Mach numbers [i.e., $p'/\bar{p} \sim -\gamma/2M^2(u'/\bar{u})^2$] (Ref. 7), the assumption is used on an ad hoc basis and remains heuristic. Laser Doppler velocimetry (LDV) is a less used alternate technique for supersonic flow.[15–18] Since LDV provides direct measurements of the velocity, the first term on the right-hand side of the Reynolds shear stress [Eq. (1)] is directly measureable. However, as Eq. (1) indicates, a number of terms remain undetermined.

The objective of the present paper is to develop an experimental procedure aimed at addressing the clearly defined requirement[2,3] for accurate supersonic turbulence data. In addition to accuracy, a supplementary condition that the data also be appropriate for turbulence model development and evaluation was imposed. Hence, to meet the research goal, a data reduction procedure for the combined usage of LDV and multiple overheat cross-wire (or, in this case, film) anemometry for the direct measurement of all of the second-order terms in Eqs. (1) and (2) for thin-layer, nonreacting, supersonic, turbulent flows, as well as attaining the mean velocity, mass flux, and density, was developed. A Mach 2.8 zero pressure gradient wall boundary layer ($Re_\theta = 1.12 \times 10^4$) was used to demonstrate the technique. Since the characteristics of supersonic, zero pressure gradient turbulent boundary layers are well understood and readily predictable with computational fluid dynamics and modern turbulence models,[19] the directly measured mean flow and turbulence data were compared with numerical predictions. Favre averaged turbulence modeling was accomplished with the k-ω formulation.[19] Reynolds averaged results were generated with the compressible apparent mass mixing length extension (CAMMLE) model.[20]

Facilities and Instrumentation

Facilities

The experiments were performed in the U.S. Air Force Institute of Technology (AFIT) supersonic wind tunnel. This blowdown, pressure-vacuum system provided 25-s test times at Mach 2.88, with a ± 0.03 variation across the test section. The settling chamber pressure and temperature were maintained at 2.0 ± 0.03 atm and 294 ± 2K for all tests. The freestream $Re/m = 17 \times 10^6$. The freestream turbulent kinetic energy was 0.016% of the mean specific kinetic energy. The test section was 6.35×6.35 cm in cross section. The coordinate system was defined such that x was positive in the streamwise direction, and the origin was located at the nozzle exit. The present measurement location was nominally 3500 momentum thickness heights (i.e., 48.0 cm) downstream of the nozzle exit. By this station, the boundary layer had reached a state of equilibrium.[18] The freestream Mach number at this downstream measurement station was 2.79.

Instrumentation

A Dantec brand 57N Enhanced BSA two-component LDV system, with a 300 mW argon-ion laser, was used for the present experiment. The $1/e^2$ beam diameter was 0.82 mm. To eliminate possible angular bias errors,[16] the green (514.5 nm) and blue (418.0 nm) beams were aligned parallel and perpendicular to the model walls, respectively. A 40 MHz frequency shift was applied across both the green and blue components. A 600-mm focal-length transmitting lens was used; this provided a 0.28-mm-diam control volume that was 0.9 cm long (along the z axis). Because of the increased intensity of the scattered light, forward scattering was used. However, to prevent damaging the photomultiplyer tubes, the system was operated at 3.5 deg off axis.

The flow was seeded by injecting atomized particles of olive oil along the centerline of the tunnel upstream of the flow straightners within the stilling chamber. The particles were generated with a TSI brand model 9306 six-jet atomizer. Based on the manufacturer's manual,[21] roughly 90% of the particles visible to their sizing apparatus (i.e., >0.5 μm) were smaller than 1.0 μm. Hence, the 3-dB point frequency response ranged from 60–200 kHz (Ref. 22).

Table 1 Overheat ratios for two wires on the cross-film probe

	1	2	3	4	5	6	7
Film 1	2.00	1.91	1.83	1.74	1.69	1.65	1.52
Film 2	2.00	1.90	1.82	1.74	1.68	1.65	1.52

The required frequency response for axial turbulence intensity was estimated for this flow at roughly 250 kHz (Refs. 7 and 10). However, the incompressible data of Klebanoff[23] indicate that the frequency response requirement is actually more stringent for axial velocity fluctuations than for the Reynolds shear stresses. From the Klebanoff[23] data, it was inferred that the magnitude of the turbulent shear stress would decrease by one to two orders of magnitude for the present range of bandwidths.[11] Thus, the expected error for the present frequency response was expected to range from 1 to 10%. The laser Doppler system was operated in burst mode at a single location for the 12.0-s portion of the steady test period. Since the data rate varied from about 0.5 kHz, near the wall, to about 3 kHz, in the freestream, the number of samples for each average varied from about 6000 to 30,000 across the boundary layer.

A TSI brand IFA 100 constant temperature anemometer system with a symmetrical bridge was used with cross-film sensors. The TSI 1243-20 cross-film probes had two cylindrical platinum film sensors each with a length of 1.0 mm and a diameter of 51 μm. The cross-film probe area was nominally 1.0 mm^2. The frequency response was optimized to nominally 150 kHz by the square wave technique in the Mach 2.79 freestream. Seven overheat ratios (Table 1) were used, where the multiple overheats were accomplished over a series of tunnel runs. To minimize frequency response limitations,[10] the lowest overheat ratio was chosen as 1.52 (lowest frequency response was approximately 90 kHz). The sampling rate was set to 10 kHz, and filtering was not performed. A total of 1024 samples were acquired at each overheat. A single overheat ($OHR = 2.0$) continuous traverse data set was also acquired. The traverse speed was set at 2.5 mm/s, and the averages were constructed over 1024 block samples of the profile.

Conventional pitot and cone static pressure probes were used to directly measure the local Mach number. The pitot probe was constructed from 1.59-mm outer diameter stainless steal tubing. The end of the tube was crimped such that the height of the opening was approximately one-half of the width. The 10 ± 0.03 deg semivertex angle cone static probe was machined out of stainless steal. Four pressure taps were located around the circumference of the probe at 90 deg intervals to minimize misalignment errors.[24] The diameter of the probe at the measurement tap location was 1.7 mm. For these data, the traverse speed was 2.5 mm/s and the sampling rate was 200 Hz.

Data Reduction

Conventional Mean Flow Pressure Probes

The Mach number was computed from the ratio of the cone static and pitot pressure using Taylor–Mccoll conical flow theory and the Rayleigh–Pitot formula. To expedite the data reduction, the following curvefit to the numerical solution was generated:

$$M = \left[-0.05298 + 4.684(p_c/p_{t2}) - 18.68(p_c/p_{t2})^2 + 50.70(p_c/p_{t2})^3 - 54.16(p_c/p_{t2})^4\right]^{-1}$$

The standard deviation for the curve was 0.06% for $M \in [1.6, 4.4]$. Random error analysis indicated a nominal 2.0% uncertainty in the Mach number. The velocity and density were estimated using thermal and calorically perfect gas relations, with the assumption of an adiabatic flow.

Cross Film

The multiple overheat cross-film (or wire) data reduction techniques developed here were founded in the analyses of Kovasznay[4] and Spangenberg.[5] In general, the reduction was based on the semi-empirical heat loss formula

$$Nu = aRe_e^n + b \tag{3}$$

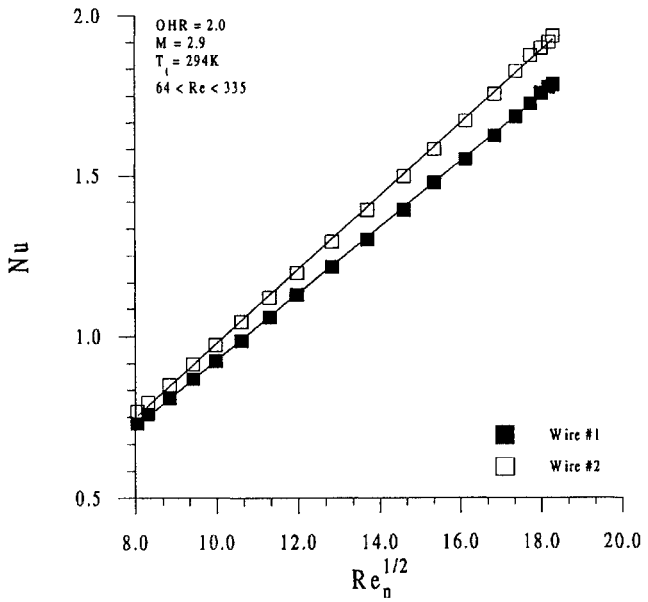

Fig. 1 Example calibration of present cross-film probes in the Mach 2.9 freestream (linear regression correlation coefficients were 0.9996 and 0.9999).

where Re_e is the effective cooling Reynolds number and the constants a and b depend on overheat ratio. The exponent n depends slightly on the wire Reynolds number and probe design[9] (typically, n is in the range of 0.4–0.55). For the present study, a value of n of 0.50 (i.e., King's law) was found to be adequate. The sensors were calibrated by placing them in the freestream and varying the tunnel total pressure. The minimum linear regression correlation coefficient for all cross-film calibrations was 0.993. Shown in Fig. 1 is an example cross-film calibration for an overheat resistance ratio of 2.0.

From bridge circuitry, the Nusselt number was related to the cross-film voltage by

$$Nu = \frac{v_w^2 R_w}{(R_w + R_L + R_S)^2} \frac{1}{\pi k_t L (T_w - T_r)}$$

For wire Reynolds numbers greater than about 20, the ratio of the recovery to total temperature (T_r/T_t) has been shown to be nearly constant at 0.96 (Ref. 6). Hence, the recovery temperature in the preceding relation can adequately be replaced by the local stagnation temperature. Further, most of the heat transfer takes place in the sensor stagnation region; thus the molecular thermal properties are also usually evaluated at the stagnation conditions.[4] Thus, with the power law functions for the thermal conductivity and viscosity, i.e.,

$$k_t = k_o(T_t/T_o)^{n_k} \qquad \text{and} \qquad \mu_t = \mu_o(T_t/T_o)^{n_\mu}$$

the hot-film response equation was written as

$$v_w^2/C_o = (T_t/T_o)^{-n_k}\left[a\sqrt{Re_{oe}}(T_t/T_o)^{-n_\mu/2} + b\right](T_w - T_t)$$

where $C_o = (R_w + R_L + R_S)^2 \pi L k_o / R_w$. The terms v_w, Re_{oe}, and T_t were all replaced by their mean plus a fluctuating component and linearized by way of the binomial theorem, which resulted in[4]

$$\frac{v_w'}{\bar{v}_w} = f\frac{Re_{oe}'}{\overline{Re}_{oe}} + g\frac{T_t'}{\bar{T}_t} \tag{4}$$

where the hot-film sensitivities were given by

$$f = \frac{1}{4}\left(1 + \frac{b}{a\sqrt{\overline{Re}_e}}\right)^{-1} \qquad \text{and} \qquad g = -\frac{\bar{T}_t}{2(T_w - \bar{T}_t)} + \frac{n_k}{2} - f n_\mu \tag{5}$$

To evaluate the sensitivities f and g, the mean flow quantities $\sqrt{(\overline{Re}_e)}$ and $\bar{T}_t$ were evaluated using the mean hot-film response equation, which was expressed as

$$\sqrt{\overline{Re}_e} + \chi_i \bar{T}_t \sqrt{\overline{Re}_e} + \psi_i \bar{T}_t = \xi_i \tag{6}$$

where $\chi_i = -1/T_{wi}$, $\psi_i = -b_i/(a_i T_{wi})$, $\xi_i = \bar{v}_{wi}^2/(C_i a_i T_{wi}) - b_i/a_i$, $C = C_o$ with k_o replaced by k_t, and i indexed the film overheat ratio. A minimum of two overheat values were required to solve for the two mean flowfield parameters in Eq. (6). However, more than two were used. Thus, a least squares analysis was applied, which yielded the following two equations:

$$N\sqrt{\overline{Re}_e} + \bar{T}_t\left(\sum \chi_i - \sum \psi_i \xi_i\right) + 2\bar{T}_t\sqrt{\overline{Re}_e}\sum \chi_i + \bar{T}_t^2 \sum \chi_i \psi_i + \bar{T}_t^2\sqrt{\overline{Re}_e}\sum \chi_i^2 = \sum \xi_i \tag{7a}$$

$$\sqrt{\overline{Re}_e}\left(\sum \psi_i - \sum \chi_i \xi_i\right) + \bar{T}_t \sum \psi_t^2 + 2\bar{T}_t\sqrt{\overline{Re}_e}\sum \chi_i \psi_i + \sqrt{\overline{Re}_e^2}\sum \chi_i + \bar{T}_t\sqrt{\overline{Re}_e^2}\sum \chi_i^2 = \sum \psi_i \xi_i \tag{7b}$$

where the summations were over the N (=7, here) overheat ratios. The solution to Eqs. (7a) and (7b) was found iteratively using the secant method, where 7–10 iterations were usually required for convergence to a normalized tolerance of 1×10^{-3}.

The turbulent flow measurements were obtained by squaring Eq. (4)

$$f_i^2\overline{\left(\frac{Re_{oe}'}{\overline{Re}_{oe}}\right)^2} + 2f_i g_i\overline{\left(\frac{Re_{oe}'T_t'}{\overline{Re}_{oe}\bar{T}_t}\right)} + g_i^2\overline{\left(\frac{T_t'}{\bar{T}_t}\right)^2} = \overline{\left(\frac{v_w'}{\bar{v}_w}\right)_i^2} \tag{8}$$

Three film temperatures were required to resolve the three turbulence terms in Eq. (8). Since more than three were used, a least squares analysis was developed by extending the normal-wire method described in Walker et al.,[13] which gave

$$\begin{bmatrix} \sum f_i^4 & 2\sum f_i^3 g_i & \sum f_i^2 g_i^2 \\ \sum f_i^3 g_i & 2\sum f_i^2 g_i^2 & \sum f_i g_i^3 \\ \sum f_i^2 g_i^2 & 2\sum f_i g_i^3 & \sum g_i^4 \end{bmatrix} \begin{Bmatrix} \overline{\left(\frac{Re_{oe}'}{\overline{Re}_{oe}}\right)^2} \\ \overline{\left(\frac{Re_{oe}'T_t'}{\overline{Re}_{oe}\bar{T}_t}\right)} \\ \left(\overline{T_t'}/\bar{T}_t\right)^2 \end{Bmatrix} = \begin{Bmatrix} \sum f_i^2\overline{\left(\frac{v_w'}{\bar{v}_w}\right)_i^2} \\ \sum f_i g_i\overline{\left(\frac{v_w'}{\bar{v}_w}\right)_i^2} \\ \sum g_i^2\overline{\left(\frac{v_w'}{\bar{v}_w}\right)_i^2} \end{Bmatrix} \tag{9}$$

Spangenberg[5] reported that if the product of the Mach number and the sine of the angle of the flow relative to the wire is greater than 1.0, then the wire (or film) response was independent of the Mach number. Further, the response was found to be a function of the normal component of the Reynolds number, that is, $Re_e = Re_n$. However, more refined angular sensitivity methods have been developed for supersonic flows.[14] For the present study, the flow angles did not substantially deviate from those of the calibration. Hence, the results of Spangenberg[5] were deemed adequate. However, the present method is readily extendable to practically any heat transfer formulation. The effective Reynolds number for each of the two films on the probe was related to the x and y components by the following:

$$Re_{ej}^2 = A_{1j}Re_x^2 + 2A_{2j}Re_x Re_y + A_{3j}Re_y^2 \tag{10}$$

where for the present cosine law formulation

$$A_{1j} = \cos^2\phi_j \qquad A_{2j} = \cos\phi_j \sin\phi_j \qquad A_{3j} = \sin^2\phi_j$$

The subscript j indexed the two "wires" on the cross-film probe, and ϕ was the angle between the x axis and the normal to the cross-film sensor. Replacing the Reynolds numbers in Eq. (10) by their mean

plus a fluctuating component, and using the binomial theorem to linearize, the mean x and y Reynolds numbers or mass flux were related to the mean effective Reynolds numbers of the two wires by

$$\overline{Re}_{ox} = \frac{\overline{\rho u} d_w}{\mu_o} = \sqrt{\frac{\overline{Re}_{oe1}^2/A_{21} - \overline{Re}_{oe2}^2/A_{22}}{A_{11}/A_{21} - A_{12}/A_{22}}}$$

$$\overline{Re}_{oy} = \frac{\overline{\rho v} d_w}{\mu_o} = \frac{1}{2\overline{Re}_x} \frac{\overline{Re}_{oe1}^2/A_{11} - \overline{Re}_{oe2}^2/A_{12}}{A_{21}/A_{11} - A_{22}/A_{12}} \tag{11}$$

where, in the derivation of Eq. (11), it was assumed that $\theta \ll 1.0$. Equation (7) was used to find the mean effective Reynolds numbers in Eq. (11) for each of the sensors on the cross-film probe.

The Cartesian mass flux fluctuating components were related to the effective Reynolds number fluctuations by

$$\left(\frac{Re'_{oe}}{\overline{Re}_{oe}}\right)_j = B_{1j}\frac{(\rho u)'}{\overline{\rho u}} + B_{2j}\frac{(\rho v)'}{\overline{\rho u}} \tag{12}$$

where $B_{1j} = A_{ij}/(A_{1j} + 2A_{2j}\theta)$ and $B_{2j} = A_{2j}/(A_{1j} + 2A_{2j}\theta)$. Squaring Eq. (12) and solving for the three turbulence unknowns yielded

$$\overline{\left[\frac{(\rho u)'}{\overline{\rho u}}\right]^2} = \frac{1}{D_2^2}\left[\frac{1}{B_{21}^2}\overline{\left(\frac{Re'_{oe}}{\overline{Re}_{oe}}\right)_1^2} - \frac{2}{B_{21}B_{22}}\overline{\left(\frac{Re'_{oe}}{\overline{Re}_{oe}}\right)_1\left(\frac{Re'_{oe}}{\overline{Re}_{oe}}\right)_2} + \frac{1}{B_{22}^2}\overline{\left(\frac{Re'_{oe}}{\overline{Re}_{oe}}\right)_2^2}\right]$$

$$\overline{\left[\frac{(\rho v)'}{\overline{\rho u}}\right]^2} = \frac{1}{D_1^2}\left[\frac{1}{B_{11}^2}\overline{\left(\frac{Re'_{oe}}{\overline{Re}_{oe}}\right)_1^2} - \frac{2}{B_{11}B_{12}}\overline{\left(\frac{Re'_{oe}}{\overline{Re}_{oe}}\right)_1\left(\frac{Re'_{oe}}{\overline{Re}_{oe}}\right)_2} + \frac{1}{B_{12}^2}\overline{\left(\frac{Re'_{oe}}{\overline{Re}_{oe}}\right)_2^2}\right] \tag{13}$$

$$\frac{\overline{(\rho u)'(\rho v)'}}{(\overline{\rho u})^2} = \frac{1}{B_{11}B_{21}}\left\{\overline{\left[\frac{Re'_{oe}}{\overline{Re}_{oe}}\right]^2} - B_{11}^2\overline{\left[\frac{(\rho u)'}{\overline{\rho u}}\right]^2} - B_{21}^2\overline{\left[\frac{(\rho v)'}{\overline{\rho u}}\right]^2}\right\}$$

where Eq. (9) was used to measure the effective Reynolds number fluctuation turbulence intensities for each film on the probe. The cross-correlation term in Eq. (31) was found by taking the covariance between the two hot-film signals, i.e.,

$$\overline{\left(\frac{Re'_{oe}}{\overline{Re}_{oe}}\right)_1\left(\frac{Re'_{oe}}{\overline{Re}_{oe}}\right)_2}\sum f_{1i}f_{2i} = \sum\overline{\left(\frac{v'_w}{\bar{v}_w}\right)_1\left(\frac{v'_w}{\bar{v}_w}\right)_2} - \overline{\left(\frac{T'_t}{\bar{T}_t}\right)^2}\sum g_{1i}g_{2i} - \overline{\left(\frac{Re'_{oe}}{\overline{Re}_{oe}}\frac{T'_t}{\bar{T}_t}\right)_1}\sum f_{1i}g_{2i} - \overline{\left(\frac{Re'_{oe}}{\overline{Re}_{oe}}\frac{T'_t}{\bar{T}_t}\right)_2}\sum f_{2i}g_{1i} \tag{14}$$

where again the summations were over the N overheat ratios.

The Cartesian mass flux total temperature correlations were related to the cross-film results by

$$\frac{\overline{(\rho u)'T'_t}}{\overline{\rho u}\bar{T}_t} = \frac{1}{D_2}\left[\frac{1}{B_{21}}\overline{\left(\frac{Re'_{oe}T'_t}{\overline{Re}_{oe}\bar{T}_t}\right)_1} - \frac{1}{B_{22}}\overline{\left(\frac{Re'_{oe}T'_t}{\overline{Re}_{oe}\bar{T}_t}\right)_2}\right]$$

$$\frac{\overline{(\rho v)'T'_t}}{\overline{\rho u}\bar{T}_t} = \frac{1}{D_1}\left[\frac{1}{B_{11}}\overline{\left(\frac{Re'_{oe}T'_t}{\overline{Re}_{oe}\bar{T}_t}\right)_1} - \frac{1}{B_{12}}\overline{\left(\frac{Re'_{oe}T'_t}{\overline{Re}_{oe}\bar{T}_t}\right)_2}\right] \tag{15}$$

The Reynolds turbulent shear stresses, Eq. (1), were related to the mass flux fluctuation correlation (i.e., the cross-film output) by the following second-order identity[25]:

$$\frac{\tau_{xy}^R}{\bar{\rho}\bar{u}^2} \equiv -\frac{\overline{(\rho u)'(\rho v)'}}{(\overline{\rho u})^2} + \frac{\bar{v}}{\bar{u}}\overline{\left(\frac{\rho'}{\bar{\rho}}\right)^2} \tag{16}$$

For thin-layer-type flows, the second term on the right-hand side is usually much smaller than the first. This was verified for the present flow, where the second term was estimated, by assuming a zero pressure fluctuation field (i.e., $p' = 0$), to be nominally 1–3% of the first. Hence for the present thin-layer, nonreacting flow, cross-wire anemometry provided a direct measurement of the full compressible Reynolds averaged shear stresses in Eq. (1).

Approximate Single Overheat Analysis

An often used simplification to the preceding multiple overheat analysis is to minimize the total temperature response by operating the probes at a high overheat ratio [Eq. (5)]. Hence for flows with reasonably small total temperature fluctuations (<3.0%), the second term on the right-hand side of Eq. (4) can be neglected, and the total temperature is assumed constant throughout the flow. Since the measured total temperature fluctuations for the present study peaked at roughly 2.0%, this method was deemed appropriate. Thus, in addition to the multiple overheat data, a single overheat data set, with improved spatial resolution, was acquired for comparative purposes.

LDV

LDV provided direct measurements of the mean velocity ($\bar{u}$) and the kinematic Reynolds shear stress {i.e., first term on the right-hand side of the Reynolds shear stress [Eq. (1)]}; that is,

$$\frac{\tau_{xy}^i}{\bar{\rho}\bar{u}^2} = -\frac{\overline{u'v'}}{\bar{u}^2} \tag{17}$$

The kinematic Reynolds shear stress is related to the Favre shear stress by the following identity:

$$\bar{\rho}\overline{u''v''} \equiv \bar{\rho}\overline{u'v'} + \bar{\rho}\overline{u''}\,\overline{v''} \tag{18}$$

where $\overline{u''_i} = -\overline{\rho' u'_i}/\bar{\rho}$. Thus for homogeneous gaseous flows, where $\rho'/\bar{\rho}$ is expected to be on the order of 1/10, the second term on the right-hand side of Eq. (5) is fourth order. Hence, the second term was neglected with respect to the second-order shear stresses.

Combined Analysis

For thin-layer flows where $\bar{v}/\bar{u} \ll 1.0$, the laser Doppler and cross-wire data can be combined to yield direct measurements of the mean transverse Favre velocity fluctuation. Hence Eqs. (1), (3), and (4) were combined to give

$$\frac{\overline{\rho' v'}}{\bar{\rho}\bar{u}} = -\frac{\overline{v''}}{U} = \frac{\overline{u'v'}}{\bar{u}^2} - \frac{\overline{(\rho u)'(\rho v)'}}{(\overline{\rho u})^2} \tag{19}$$

Thus, the turbulent mass flux in Eq. (1) was measured. Although the turbulent mass flux does not appear explicitly in Eq. (2), it is also important to Favre averaged based analyses. For example, it does appear directly as pressure work in the transport of the Favre turbulent shear stress and turbulent kinetic energy.[19]

Following the same procedure used to derive Eqs. (16) and (19), the Reynolds and Favre averaged turbulent heat flux was related to the measurable quantities by the following two identities:

$$\frac{q_y^R}{\bar{\rho}\bar{u}C_p\bar{T}_t} = \frac{\overline{(\rho v)'T'_t}}{\overline{\rho u}\bar{T}_t} + \frac{\overline{\rho' v'}}{\bar{\rho}\bar{u}} \qquad \frac{q_y^F}{\bar{\rho}UC_p\bar{T}_t} = \frac{\overline{(\rho v)'T'_t}}{\overline{\rho u}\bar{T}_t} \tag{20}$$

Hence, all of the turbulence terms appearing in either the Favre or Reynolds averaged Navier–Stokes equations were measured via the present combined LDV/cross-film analysis.

In addition to the turbulence quantities described earlier, the LDV/cross-film mean flow results were also combined to provide an estimate of the mean density:

$$\bar{\rho} = \frac{\overline{\rho u}}{\bar{u}} - \frac{\overline{\rho' u'}}{\bar{u}} \tag{21}$$

where the second-order turbulence correlation on the right-hand side of Eq. (21) was neglected with respect to the zeroth-order terms.

Numerical Methods

As mentioned in the Introduction, the present flowfield is manageable with current computational techniques. Thus, two cell-centered, finite volume, two-dimensional Navier–Stokes computational codes written in generalized curvilinear coordinates were used as a means of qualitatively evaluating the present data. First, the code described in Gaitonde and Shang[26] was modified by Fick et al.[27] to include the k-ω turbulence model.[19] Since the formulation described in Wilcox[19] was developed for the Favre averaged Navier–Stokes equations, it was used to evaluate the measured Favre averaged turbulence data [Eq. (2)]. All k-ω solutions were converged such that the normalized residual was less than 10^{-9} (Ref. 27). Detailed studies to ensure grid independence were also performed (see Fick et al.[27]). The zero pressure gradient solution for that study was started with measured data that was acquired 20.5 cm downstream of the nozzle exit. Numerical profiles were presented for a station that was 36.5 cm downstream of the nozzle exit, which was 11.5 cm upstream of the present measurement station. However, because the flow was in equilibrium,[18] the reported numerical solutions were suitable for profile shape comparisons.

To predict the Reynolds averaged turbulence properties [Eq. (1)], a cell-centered parabolized Navier–Stokes code was written that incorporated the CAMMLE model.[20] The CAMMLE model was coded as described in Bowersox and Schetz.[20] However, for an adiabatic flow, the strong Reynolds analogy and the Crocco integral were used to show that the model constant S should be unity. The turbulent Prandtl number and wall temperature were both held constant at 0.9 and 280 K, respectively. The solutions were obtained on a 30.0 × 5.0 cm numerical domain. As in the Fick et al.[27] study, the inflow condition was generated from the experimental data acquired 20.5 cm downstream of the nozzle exit. Two grids were used: a coarse grid and fine grid with 50 × 50 and 100 × 100 nodes, respectively. For the fine grid, the first grid point was located at a distance that corresponded to a y^+ value that was estimated to be 1.0 (i.e., 7×10^{-6} m); for the coarse grid, that distance was doubled. The normalized L_2 residual was reduced by three orders of magnitude on each plane. The differences between the fine and coarse grid solutions were indistinguishable (see Fig. 2). Therefore, only the fine grid results are compared with the experimental data.

Supersonic Boundary-Layer Results

The wall boundary layer in the AFIT supersonic pressure-vacuum blowdown wind tunnel was used to evaluate the present data reduction techniques. The measurements were obtained at approximately 48.0 cm (3500 boundary-layer momentum thickness heights) downstream of the nozzle exit. The boundary-layer characteristics and freestream edge conditions are summarized in Table 2. The agreement between the measured (9.85 mm) and CAMMLE model prediction (9.92 mm) of the boundary-layer height was excellent.

In Fig. 3, the LDV (closed squares) mean velocity results are compared with those estimated from the conventional pitot and cone static pressure data (open squares). As indicated, the two techniques agreed very well, except for $y/\delta < 0.15$, where it is expected that the relatively large size of the conventional probes resulted in discrepancy near the wall. The cross-film mass flux measurements (closed diamonds) were also compared with estimates from the conventional probe data (open diamonds). The agreement was again very good. However, the cross-film data point at $y/\delta = 0.13$ was about 20% higher; again, the result of a probe volume induced error. The density measurements [closed triangles, Eq. (21)] are also in good agreement with the conventional probe data (open triangles). Note that because this was a measurement technique investigation, the multiple overheat cross-film profiles consisted of only five data points across the boundary layer. Random error estimates, which accounted for probe position uncertainty, calibration errors, flow repeatability, and sample size, for all of the acquired data, are summarized in Table 3. Also shown in Fig. 3 are the results from the

Table 2 Boundary-layer conditions

M_e	u_e, m/s	ρ_e, kg/m^3	δ, mm	δ_k^*, mm	δ^*, mm	θ_k, mm	Re_θ
2.79	602.0	0.24	9.85	0.62	1.27	0.50	1.12×10^4

Table 3 Random error uncertainty estimates

Measurement	Eq.	Unc., %	Fig.
Velocity (LDV)	NA[a]	4.0	3
Mass flux (cross-film)	NA	3.0	3
Density	21	7.0	3
Velocity (conv. probe)	NA	1.5	3
Mass flux (conv. probe)	NA	2.1	3
Density (conv. probe)	NA	3.6	3
Reynolds shear stress	16	9.0	4
Favre shear stress	18	8.0	4
Reynolds apparent mass	19	17.0	5
Reynolds heat flux	20	26.0	6
Favre heat flux	20	9.0	6

[a]NA = not applicable.

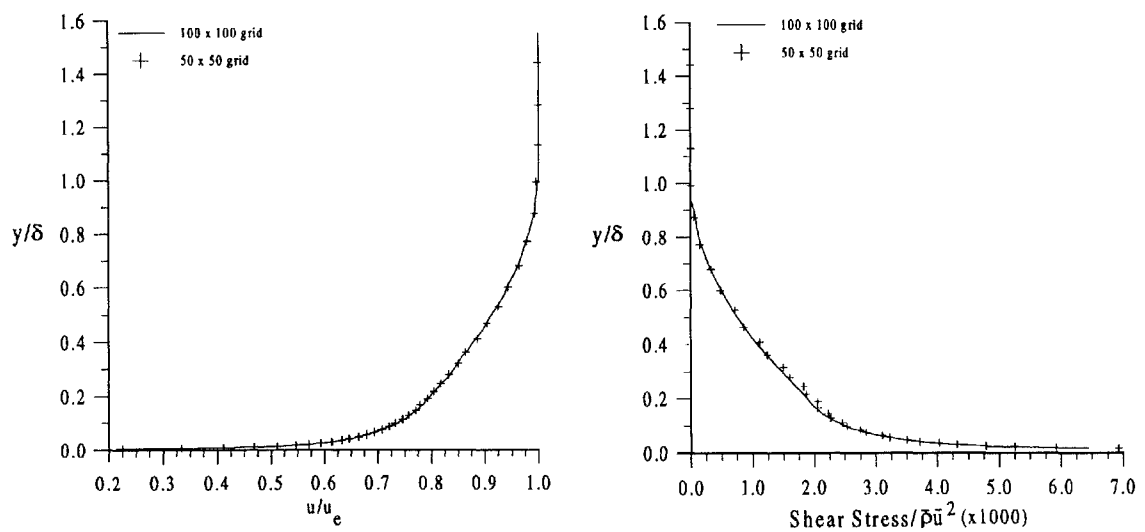

a) Mean velocity

b) Favre turbulent shear stress

Fig. 2 Grid comparison for the numerical predictions using the CAMMLE turbulence model.

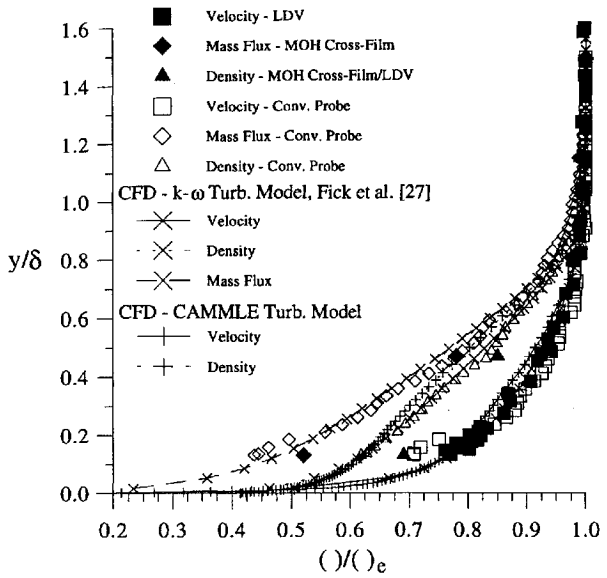

Fig. 3 Measured mean velocity, mass flux, and density, with comparison to conventional probe results and numerical predictions with the k-ω and CAMMLE turbulence models.

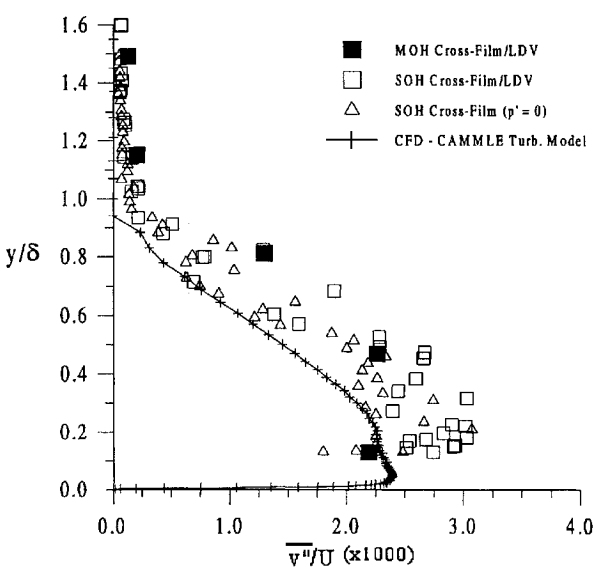

Fig. 5 Measured mean transverse Favre averaged velocity fluctuation component, with comparison to a numerical prediction with the CAMMLE turbulence model.

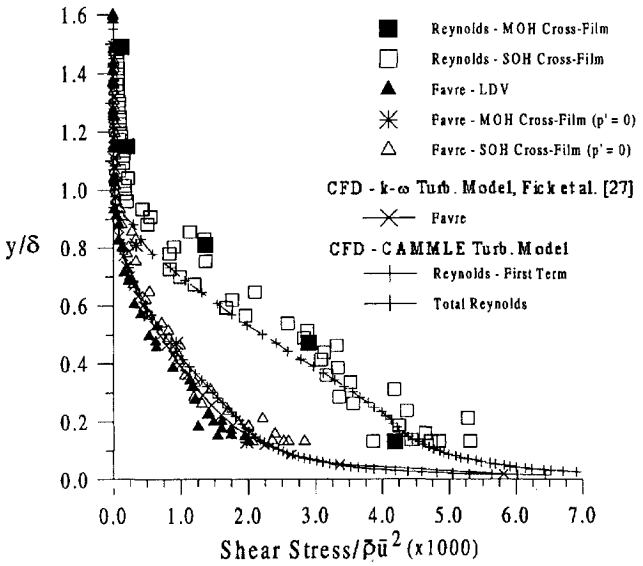

Fig. 4 Measured Reynolds and Favre averaged shear stress profiles, with comparisons to numerical predictions with the k-ω and CAMMLE turbulence models.

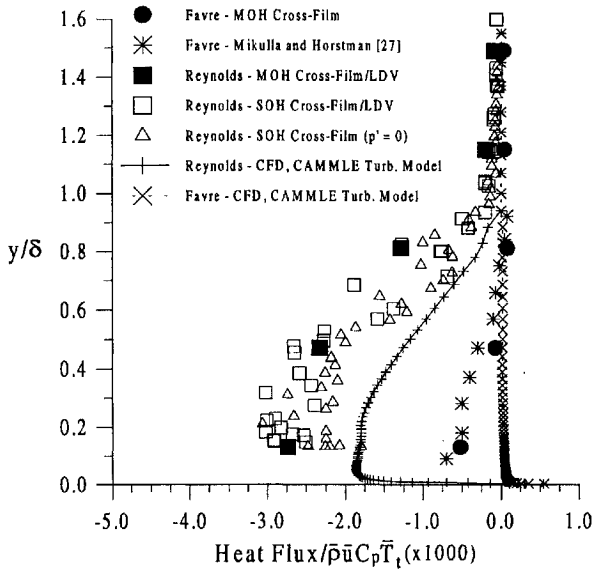

Fig. 6 Measured Reynolds and Favre averaged turbulent heat flux profiles, with comparison to numerical predictions with the CAMMLE turbulence model.

computational fluid dynamics analyses. As can be seen, the results from both models agreed well with the experimental data.

The turbulent shear stress results are shown in Fig. 4. The Reynolds shear stresses [Eq. (16)] were measured with both the multiple (closed squares) and single overheat (open squares) cross-film methods. Agreement between the two methods was excellent. The directly measured Favre shear stresses [Eqs. (17) and (18); Fig. 4, closed triangles] measured with the LDV were compared with those estimated from the single (open triangles) and multiple (asterisks) overheat cross-film data using the assumption that $p' = 0$. As expected, the static pressure fluctuation assumption did appear to be adequate for the present flow.[7] The k-ω Favre shear stress prediction was also in excellent agreement with the LDV measurements. The CAMMLE formulation, which modeled each of the terms in Eq. (1) for a thin-layer flow, predictions of the first term ($-\bar{\rho}\widetilde{u'v'}$) and total Reynolds shear stress were also in very good agreement with the measurements.

The mean transverse Favre velocity fluctuation (i.e., the turbulent apparent mass) estimated from the LDV and cross-film data with Eq. (19) are given in Fig. 5. Since the evaluation of Eq. (19) required both the LDV and cross-film data, the difference between the locations of the data point positions across the profile used in the analysis was maintained to within ±0.1 mm. As shown, the single (open squares) and multiple (closed squares) overheat results were in reasonable agreement with each other. In addition, the estimates obtained from the single overheat data and the $p' = 0$ assumption (open triangles) agreed with the direct measurements. The CAMMLE model predictions were also in reasonable agreement with the measurements.

The Reynolds and Favre transverse turbulent heat flux results [Eq. (20)] are plotted in Fig. 6. The directly measured Favre results (closed circles) are compared with the hypersonic boundary-layer data of Mikulla and Horstman.[28] As indicated, the results from the two experiments compare favorably. The agreement between the various measurement methods for the Reynolds heat flux was again very good. When compared with the turbulent shear stress (Fig. 4) and apparent mass (Fig. 5), the agreement between the CAMMLE model prediction and the measurements was relatively poor. A different choice for the turbulent Prandtl number may have improved the numerical prediction.

As Figs. 3–6 and Table 3 demonstrate, the present data reduction techniques can be used to acquire with a reasonable degree of accuracy all of the second-order turbulence terms in both the Reynolds or Favre averaged forms of the Navier–Stokes equations for thin-layer, nonreacting, supersonic turbulent flows. The techniques developed earlier are also readily extendible to three-dimensional, thin-layer flows.

Conclusions

A detailed analysis of the combined usage of laser Doppler velocimetry and multiple overheat cross-wire anemometry for the direct measurement of both the mean and turbulent flow properties of supersonic flow that are appropriate for turbulence model evaluation and development was presented. In particular, a technique for the direct measurement of all of the second-order turbulence correlation terms appearing in either the Reynolds or Favre averaged Navier–Stokes equations, for thin-layer nonreacting flow, was developed. A Mach 2.8 zero pressure gradient turbulent boundary layer was chosen as a test case. This choice was based on the knowledge that the accuracy of current experimental methods and modern computational techniques for this type of flow has been well established. The agreement between the present direct measurements to estimates based on the more conventional techniques and to numerical predictions (k-ω and CAMMLE turbulence models) was considered excellent.

Acknowledgment

The author gratefully acknowledges James McMichael of the U.S. Air Force Office of Scientific Research for sponsoring this work.

References

[1]Morkovin, M., "Effects of Compressibility on Turbulent Flows," *The Mechanics of Turbulence*, AGARD, Gordon and Breach, New York, 1961, pp. 368–380.

[2]Spina, E., Smits, A., and Robinson, S., "The Physics of Supersonic Turbulent Boundary Layers," *Annual Review of Fluid Mechanics*, Vol. 26, 1994, pp. 287–319.

[3]Settles, G., and Dodson, L., "Supersonic and Hypersonic Shock/Boundary-Layer Interaction Database," *AIAA Journal*, Vol. 32, No. 7, 1994, pp. 1377–1383.

[4]Kovasznay, L. S. G., "The Hot-Wire Anemometry in Supersonic Flow," *Journal of the Aeronautical Sciences*, Vol. 17, Sept. 1950, pp. 565–584.

[5]Spangenberg, W. G., "Heat Loss Characteristics of Hot-Wire Anemometers at Various Densities in Transonic and Supersonic Flow," NACA TN 3381, May 1955.

[6]Laufer, J., and McClellan, R., "Measurements of Heat Transfer from Fine Wire in Supersonic Flow," *Journal of Fluid Mechanics*, Vol. 1, 1956, pp. 276–289.

[7]Kislter, A., "Fluctuation Measurements in a Supersonic Turbulent Boundary Layer," *Physics of Fluids*, Vol. 2, No. 3, 1959, pp. 290–296.

[8]Demetriades, A., and Laderman, A., "Reynolds Stress Measurements in a Hypersonic Boundary Layer," *AIAA Journal*, Vol. 11, No. 11, 1973, pp. 1594–1596.

[9]Smits, A., Hayakawa, K., and Muck, K., "Constant Temperature Anemometer Practice in Supersonic Flows, Part 1: The Normal Wire," *Experiments in Fluids*, Vol. 1, No. 2, 1983, pp. 83–92.

[10]Bestion, D., Gaviglio, J., and Bonnet, J., "Comparison Between Constant-Current and Constant-Temperature Hot-Wire Anemometers in High-Speed Flows," *Review of Scientific Instruments*, Vol. 54, No. 11, 1983, pp. 1513–1524.

[11]Hinze, J., *Turbulence*, 2nd ed., McGraw–Hill, New York, 1975.

[12]Logan, P., McKenzie, R., and Bershader, D., "Hot-Wire Accuracy in Supersonic Turbulence from Comparisons with Laser-Induced Fluorescence," *AIAA Journal*, Vol. 26, No. 3, 1987, pp. 316–322.

[13]Walker, D., Ng, W., and Walker, M., "Experimental Comparison of Two Hot-Wire Techniques in Supersonic Flow," *AIAA Journal*, Vol. 27, No. 8, 1989, pp. 1074–1080.

[14]Donovan, J., and Spina, E., "An Improved Analysis of Method for Cross-Wire Signals Obtained in Supersonic Flow," *Experiments in Fluids*, Vol. 12, No. 6, 1992, pp. 359–368.

[15]Johnson, D., and Rose, W., "Laser Velocimeter and Hot-Wire Anemometer Comparison in a Supersonic Boundary Layer," *AIAA Journal*, Vol. 13, No. 4, 1975, pp. 512–515.

[16]Robinson, S. K., Seegmiller, H. L., and Kussoy, M. I., "Hot-Wire and Laser Doppler Velocimetry Measurements in a Supersonic Boundary Layer," AIAA Paper 83-1723, July 1983.

[17]Elena, M., and LeCharme, J., "Experimental Study of Supersonic Turbulent Boundary Layer Using a Laser Doppler Anemometer," *Journal of Theoretical and Applied Mechanics*, Vol. 7, No. 2, 1988, pp. 175–190.

[18]Bowersox, R., and Buter, T., "Mass-Weighted Turbulence Measurements in a Mach 2.9 Boundary Layer Including Mild Pressure Gradients," AIAA Paper 96-0659, Jan. 1996; see also *AIAA Journal* (to be published).

[19]Wilcox, D., *Turbulence Modeling for CFD*, DCW Industries, Inc., La Cañada, CA, 1993.

[20]Bowersox, R., and Schetz, J., "Model for Compressible Turbulence in Hypersonic Wall Boundary and High-Speed Mixing Layers," *AIAA Journal*, Vol. 32, No. 7, 1994, pp. 1531–1533.

[21]Anon., *TSI Model 9306 Six-Jet Atomizer Instruction Manual*, TSI, Inc., St. Paul, MN, 1987.

[22]Menon, R., and Lai, W., "Key Considerations in the Selection of Seed Particles for LDV Measurements," 4th International Conf. on Laser Anemometry, Cleveland, OH, Aug. 1991.

[23]Klebanoff, P., "Characterization of the Turbulence in a Boundary Layer with Zero Pressure Gradient," NACA Rept. 1247, May 1955.

[24]Volluz, R., *Handbook of Supersonic Aerodynamics, Section 20, Wind Tunnel Instrumentation and Operation*, Ordnance Aerophysics Lab., NAVORD Rept. 1488, Vol. 6, Daingerfield, TX, Jan. 1991.

[25]Bowersox, R., and Schetz, J., "Compressible Turbulence Measurements in a High-Speed High Reynolds Number Mixing Layer," *AIAA Journal*, Vol. 32, No. 4, 1994, pp. 758–764.

[26]Gaitonde, D., and Shang, J., "The Performance of Flux-Split Algorithms in High-Speed Viscous Flow," AIAA Paper 92-0186, Jan. 1992.

[27]Fick, E., Gaitonde, D., and Buter, T., "Numerical Simulation of a Supersonic Boundary Layer with Mild Pressure Gradient," AIAA Paper 96-2059, July 1996.

[28]Mikulla, V., and Horstman, C., "Turbulence Stress Measurements in a Nonadiabatic Hypersonic Boundary Layer," *AIAA Journal*, Vol. 13, No. 12, 1975, pp. 1607–1613.